

Osteoblast-specific Knockout of the Insulin-like Growth Factor (IGF) Receptor Gene Reveals an Essential Role of IGF Signaling in Bone Matrix Mineralization*

Received for publication, August 13, 2002, and in revised form, September 3, 2002
Published, JBC Papers in Press, September 4, 2002, DOI 10.1074/jbc.M208265200

Mei Zhang‡, Shouhong Xuan§, Mary L. Bouxsein¶, Dietrich von Stechow¶, Nagako Akeno‡, Marie Claude Faugere||, Hartmut Malluche||, Guisheng Zhao‡, Clifford J. Rosen**, Argiris Efstratiadis§, and Thomas L. Clemens‡ ‡‡

From the ‡Department of Medicine, University of Cincinnati, Cincinnati, Ohio 45267, the §Department of Genetics and Development, Columbia University, New York, New York 10032, the ¶Orthopedic Biomechanics Laboratory, Beth Israel Deaconess Medical Center, Boston, Massachusetts 02215, the ||Department of Medicine, University of Kentucky, Lexington, Kentucky 40536, and the **Maine Center for Osteoporosis Research and Education, St. Joseph's Hospital, Bangor, Maine 04401

To examine the local actions of IGF signaling in skeletal tissue in a physiological context, we have used Cre-mediated recombination to disrupt selectively in mouse osteoblasts the gene encoding the type 1 IGF receptor (*Igf1r*). Mice carrying this bone-specific mutation were of normal size and weight but, in comparison with normal siblings, demonstrated a striking decrease in cancellous bone volume, connectivity, and trabecular number, and an increase in trabecular spacing. These abnormalities correlated with a striking decrease in the rate of mineralization of osteoid that occurred despite an unexpected osteoblast and osteoclast hyperactivity, detected from the significant increments in both osteoblast and erosion surfaces. Our findings indicate that IGF1 is essential for coupling matrix biosynthesis to sustained mineralization. This action is likely to be particularly important during the pubertal growth spurt when rapid bone formation and consolidation are required.

Body size and linear bone growth in mammals is affected by cellular signaling pathways controlled by growth factors and hormones (1). In this regard, a major growth-promoting signaling system consisting of the insulin-like growth factors (IGF,¹ IGF1 and IGF2) and the type 1 IGF receptor (IGF1R) regulates embryonic growth, as shown by gene knockout experiments in mice (1). IGF1 acting through IGF1R also plays central roles in postnatal growth either independently or by mediating growth hormone functions (2). Signaling through the IGF1R tyrosine kinase receptor not only promotes cell proliferation, but also mediates anti-apoptotic actions (3, 4). The IGF system includes a second receptor (IGF2R) devoid of signaling properties, but serving IGF2 turnover, and at least six IGF-binding proteins

(IGFBPs) of obscure functional significance (single and also some double mouse mutations ablating IGFBPs have not revealed as yet significant consequences in growth impairment).² The IGFs are produced locally in various tissues, including bones, and exert autocrine/paracrine functions, but they are also present in serum, mostly associated with IGFBPs. Whether the circulating IGFs act systemically as hormones is currently controversial (5, 6).

A number of *in vitro* and *in vivo* studies are progressively unraveling the significance of the IGF system for skeletal development and metabolic control (for a review see Ref. 7). IGF1, by stimulating the proliferation of chondrocytes in the growth plate, plays an essential role in longitudinal bone growth (2) and is also involved in the formation of trabecular bone. In fact, chondrocytes and bone cells produce IGFs and express IGF1R (see for example Refs. 8 and 9). Studies using osteoblast culture systems have shown that IGF1 stimulates osteoblast proliferation, accelerates their differentiation, and enhances bone matrix production (10, 11). In addition, IGF1 is being recognized as a critical factor for bone cell survival (12–14). Finally, IGF1 also appears to regulate bone resorption, either directly or through its action on osteoblasts that stimulate in turn the formation and function of osteoclasts (15).

Because of complex relationships in the signaling processes of the IGF regulatory system (1) on one hand, and intricacies in bone development (16, 17) on the other, it has been quite difficult to define individual *in vivo* aspects of the skeletal actions of IGF1, especially those brought about by local (autocrine/paracrine) mechanisms. Nevertheless, progress is being made with the use of genetically modified mice. For example, mice with targeted overexpression of IGF1 in osteoblasts exhibited an increased bone formation rate and increased trabecular and cortical bone volume (18). Remarkably, these changes occurred without an increase in the total number of osteoblasts, suggesting that locally produced IGF1 could exert its anabolic effects primarily by increasing the performance of resident osteoblasts. Nevertheless, firm establishment of causal relationships necessitates complete ablation of IGF signaling by elimination of IGF1R function. In this regard, however, the invariable neonatal lethality of *Igf1r* nullizygous mice (19) precluded an examination of the skeletal role of IGF1 during postnatal growth and development. To circumvent this problem, we have now disrupted selectively the *Igf1r* gene in

* This work was supported by a Merit Review Grant from the Veterans Administration (to T. L. C.) and National Institutes of Health Grant CA75553 (Project 3) (to A. E.). The costs of publication of this article were defrayed in part by the payment of page charges. This article must therefore be hereby marked "advertisement" in accordance with 18 U.S.C. Section 1734 solely to indicate this fact.

‡‡ To whom correspondence should be addressed: Division of Endocrinology and Metabolism, Vontz Center for Molecular Studies, 3125 Eden Ave., Cincinnati, OH 45267-0547. Tel.: 513-558-0454; E-mail: clementl@UC.edu.

¹ The abbreviations used are: IGF, insulin-like growth factor; PBS, phosphate-buffered saline; X-gal, 5-bromo-4-chloro-3-indolyl- β -D-galactopyranoside; AP, alkaline phosphatase.

² J. Pintar, personal communication.

mouse osteoblasts using the *cre/loxP* recombination system, and evaluated the bone phenotype. As we report here, this site-specific ablation of IGF signaling impairs the rate of bone formation and severely retards mineralization of osteoid resulting in decreased cancellous bone volume and altered trabecular structure.

MATERIALS AND METHODS

Generation of OC-cre Mice—A DNA fragment representing the human osteocalcin (OC) promoter (20) was cloned into the pBluescript SK(-) vector to create pOC. A plasmid containing a cDNA encoding *cre*, which was modified to include a nuclear localization sequence and the human β -actin 3'-untranslated region (provided by Dr. Thomas Doetschman, University of Cincinnati), was cloned into the pKbPa plasmid (18) downstream from a sequence representing the rabbit β -globin second intron flanked by remnants of truncated exons. The derived fused (globin-*cre*) sequences were then subcloned into pOC downstream from the osteocalcin promoter, to create pOC-*cre* (Fig. 1A). The insert of this plasmid (OC-*cre*) was excised and microinjected into fertilized eggs (FVB-N mouse strain). Transgenic lines were established from 11 founders that were identified by Southern analysis of genomic DNA. Two of the transgenic lines (4 and 6) were analyzed in detail and used in our experiments (see "Results"). Differences in the level and specificity of transgenic expression between the two lines were not detected. Expression of *cre* mRNA was determined by Northern analysis of total RNA (10 μ g per lane) using a *cre* cDNA probe. All animals received humane care in compliance with the local Institutional Animal Care and Use Committee.

Mouse Crosses—OC-*cre* mice were mated with homozygous conditional mutants carrying modified *Igf1r* alleles (with *loxP* sites flanking exon 3; (21), to generate OC-*cre*/Igf1r^{lox/+} progeny, which were used in subsequent crosses (see "Results"). The OC-*cre* mice were also crossed with Z/AP reporter mice (22), to estimate the efficiency of Cre-mediated recombination (see "Results").

Genotyping—For routine genotyping of progeny, the *cre* transgene was detected by PCR (1 min at 94 °C, 1 min at 53 °C, and 1 min at 72 °C, for 30 cycles) using the primers: 5'-CAAATAGCCCTGGCAGATTC-3' (forward) and 5'-TGATACAAGGGACATCTTCC-3' (reverse) to generate a 260-bp product corresponding to a portion of the OC promoter and the rabbit β -globin intron. The *Igf1r* locus was detected by PCR (1 min at 94 °C, 1 min at 61 °C, and 1 min at 72 °C, for 30 cycles) with the primers 2 and 3 (see Fig. 1): 5'-CTTCCAGCTTGCTACTCTAGG-3' (forward) and 5'-CAGGCTTGCAATGAGACATGGG-3' (reverse), which generate a 120-bp product from the wild-type allele or a 220-bp product from the floxed allele. To detect the recombined allele, another primer (primer 1; Fig. 1) 5'-TGAGACGTAGCGAGATTGCTGTA-3' was used in combination with primer 3, to generate a 320-bp product. Whole-mount lacZ staining was used to genotype the Z/AP reporter mice, as described below.

Determination of Cre-mediated Recombination Efficiency—To determine the specificity and efficiency of Cre-mediated recombination, OC-*cre* mice from two Cre-expressing lines (3 and 6) were crossed with the Z/AP mice (17) carrying a "double reporter" transgene (see Fig. 2A and "Results"). When recombination occurs, the *LacZ* site is excised, and the downstream human *Hplap* gene is expressed. Mice were sacrificed and organs were harvested, rinsed in PBS, and fixed with 2% paraformaldehyde plus 0.2% glutaraldehyde in PBS on ice for 2 h. For whole-mount staining, each calvarium was cut in half longitudinally, one half was used for lacZ staining and the other for AP as described (22). For lacZ staining, the fixed samples were washed three times for 5 min in lacZ wash buffer (2 mM MgCl₂, 0.01% sodium deoxycholate, 0.02% Nonidet-P40, 5 mM EGTA in PBS). Staining was carried out in lacZ staining buffer (1 mg/ml X-gal, 5 mM potassium ferrocyanide, and 5 mM potassium ferricyanide in lacZ wash buffer) at 37 °C for 4 h to overnight, with shaking and protection from light. After staining, samples were rinsed with PBS, post-fixed in 2% glutaraldehyde and 2% paraformaldehyde in 0.1 M sodium cacodylate buffer (pH 7.3) for 10 min, rinsed twice with PBS, and then twice with 70% ethanol prior to storage in 70% ethanol at 4 °C. For alkaline phosphatase (AP) staining, the fixed calvaria were washed three times with PBS for 5 min, and then incubated in PBS at 70–75 °C for 30 min to inactivate endogenous AP. Samples were rinsed in PBS, washed in AP buffer (100 mM Tris-HCl, pH 9.5, 50 mM MgSO₄, 0.01% sodium deoxycholate, 0.02% Nonidet-P40) for 10 min, and stained with NBT/BCIP stain (0.4 mg/ml NBT (nitroblue tetrazolium chloride), 0.19 mg/ml BCIP (5-bromo-4-chloro-3-indolyl-phosphate, toluidine-salt), in AP buffer) for at least 90 min or until staining was evident. After staining, samples were washed in PBS

and 70% ethanol and stored in 70% ethanol. Stained calvaria halves were dehydrated, infiltrated and embedded in paraffin. Blocks were sectioned at 10 μ m, placed onto slides, and coverslipped.

Non-skeletal tissues were sectioned prior to staining. Samples were washed in PBS three times for 5 min after fixation and cryoprotected in 15% sucrose in PBS for 1 h at 4 °C and then in 30% sucrose in PBS overnight at 4 °C. They were then embedded in OCT, sectioned, and placed onto slides. Prior to staining, slides were refixed in cold PBS containing 0.2% glutaraldehyde for 10 min. For lacZ staining, slides were washed three times for 5 min in lacZ wash buffer and then stained in lacZ staining buffer for 3–4 h at 37 °C, protected from light. After staining, slides were rinsed in PBS, postfixed (see above) before dehydration through a graded ethanol series and coverslipped. For AP staining, after fixation, slides were washed three times in PBS for 5 min and endogenous AP was inactivated by incubating slides in PBS at 75 °C for 30 min. Slides were then rinsed with PBS, washed in AP buffer for 10 min, and stained with NBT/BCIP stain for 5–15 min at room temperature. After staining, slides were washed in PBS, dehydrated through an ethanol series, and then coverslipped.

Micro CT Analysis—The three-dimensional microarchitecture of the intact right femurs was evaluated using a high-resolution, desktop microtomographic imaging system (μ CT20, Scanco Medical AG, Bassersdorf, Switzerland) (23). Three regions were evaluated: the entire femur, cortical bone in the mid-diaphysis, and secondary spongiosa in the distal metaphysis. For evaluation of the entire femur and mid-diaphyseal cortical bone, the bone was scanned using a 34- μ m slice increment, requiring ~100–150 μ CT slices per specimen. For evaluation of the secondary spongiosa in the distal metaphysis, the bone was scanned using a 9- μ m slice increment, beginning approximately at the growth plate and extending proximally for 200 CT slices. A region of interest including only cancellous bone was constructed, beginning 0.25 mm proximal to the growth plate and extending proximally for 1.25 mm. Images were reconstructed, filtered, and thresholded as previously described (24). The images were stored in three-dimensional arrays with an isotropic voxel size of either 34 μ m (for the whole bone) or 9 μ m (for the distal femoral metaphysis). Morphometric parameters were computed using a direct three-dimensional approach that does not rely on any assumptions about whether the underlying structure is either plate or rod-like (25). For the whole bone, we computed the total bone volume (BV, mm³) and the apparent volume density (AVD, %), defined as the percent of mineralized tissue volume divided by the total volume defined by the external bone envelope (24). For the cortical region, the bone volume (BV, mm³), bone volume density (BV/TV, %), and cortical thickness (μ m) were computed in a 1-mm thick region at the mid-diaphysis. For the cancellous bone region in the distal metaphysis, bone volume density (BV/TV, %), trabecular thickness (Tb.Th, μ m), trabecular separation (Tb.Sp, μ m), trabecular number (Tb.N, mm⁻³), and connectivity density (mm⁻³) were assessed.

Mineralized Bone Histology and Bone Morphometry—Distal femora and calvaria were fixed in 100% ethanol. After dehydration, bone samples were embedded in methyl methacrylate (26), and 4- μ m sections were cut with a heavy-duty microtome (Microm, C. Zeiss, Thornwood, NY). This thickness allows analysis of the same histologic features in slides prepared for light and fluorescent microscopy. Four bone sections were stained using the modified Masson-Goldner trichrome technique (27), and four others serial to the stained sections were left unstained for fluorescent microscopy.

Static and dynamic parameters of bone structure, formation, and resorption were measured using a semi-automatic method (Osteoplan II, Kontron, Munich, Germany) (18, 28). In 6-week-old mice, measurements were confined to the secondary spongiosa of the distal femur to ensure that only remodeling sites were analyzed. In 3-week-old mice, measurements were made in the epiphysis due to the lack of sufficient trabecular bone in the secondary spongiosa. For dynamic endpoints, 3- and 6-week-old animals were injected with calcein intraperitoneally on days 1 and 4 and sacrificed 2 or 3 days later. All parameters comply with the recommendations of the Histomorphometry Nomenclature Committee of the American Society of Bone and Mineral Research (29).

Statistical Analysis—Results are expressed as mean \pm S.E. All statistical tests were two-sided. An assigned significance level of 0.05 was used. Comparability of the two groups at any given time was assessed using the Mann-Whitney *U* test. Comparability of data from a group at different time points was done using the Kruskal-Wallis *H* test. All computations were performed using the SPSS software package for Windows release 7.5 (SPSS, Chicago, IL).

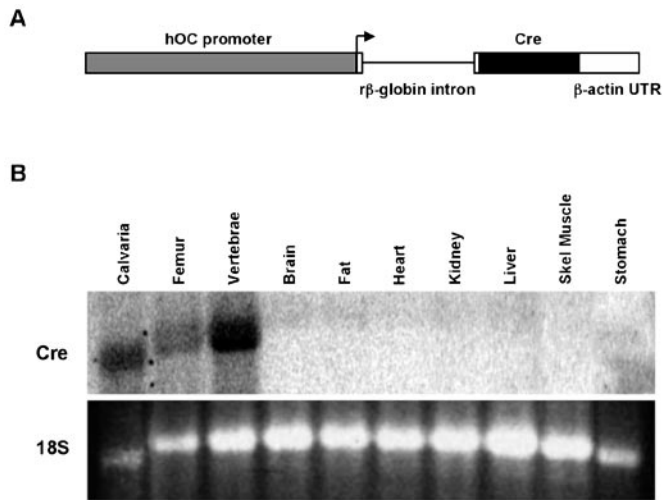


FIG. 1. **Development of Cre-expressing transgenic mice.** *A*, diagram of the human osteocalcin (hOC) DNA construct used to generate mouse lines carrying a Cre transgene. Cloning of this construct is described under “Materials and Methods.” The arrow indicates the transcriptional orientation. *B*, Northern blot analysis of OC-Cre transgene expression in tissues from Cre-expressing mice (line 6). Ten micrograms of total RNA were gel separated, transferred to a nylon membrane, and then hybridized with a Cre cDNA (top panel). The ethidium bromide staining of 18 S ribosomal RNA is shown in the bottom panel.

RESULTS

Experimental Design—Tissue-specific conditional mutagenesis requires crosses between Cre-producing and Cre-responding strains of mice. Responders used in this study, in which exon 3 of the *Igf1r* gene is “floxed” (flanked by *loxP* sites in direct orientation), have been described previously (21). To drive *cre* expression in the osteoblasts of producer mice, we used the osteocalcin (OC) gene promoter and generated OC-*cre* transgenic mice (see “Materials and Methods”). Northern analysis demonstrated that the transgene encoding the recombinase was expressed in bones and in no other of the examined tissues (Fig. 1B).

Osteoblast-specific Cre-mediated Recombination—For the purposes of our experiments, it was important to demonstrate the specificity and efficiency of Cre-mediated recombination in osteoblasts. However, the floxed *Igf1r* allele could not serve itself as a reporter for this purpose, because the heterogeneity of skeletal tissue constituents precluded an assessment of the level of DNA excision by Southern analysis (osteoblasts represent only a minor bone component). Also unsuitable were (feasible, but difficult for bone tissue) alternative analyses, such as *in situ* hybridization and immunohistochemistry, since quantitative results could not be obtained. For these reasons, we used an indirect approach and crossed OC-*cre* producers with Z/AP mice (17) carrying a “double reporter” transgene, which consists of a sequence (β geo) encoding β -galactosidase and a selectable marker flanked by two *loxP* sites that is followed by a human placental alkaline phosphatase (*hPLAP*) gene (Fig. 2A). The latter gene is expressed after Cre-mediated excision of β geo. Thus, the efficiency of Cre action can be estimated by determining in various tissues the reduction in X-gal staining and the appearance of staining for alkaline phosphatase.

To determine the time of commencement of the OC-*cre* transgene expression during development, whole calvaria harvested from OC-*cre*/Z/AP embryos were stained for AP. As shown in Fig. 2B, AP-positive cells were first detected in E17 calvaria at the primary ossification centers. Examination of sections from these calvaria revealed that the AP-positive elements were osteoblasts and osteocytes (Fig. 2C). Such sections were also

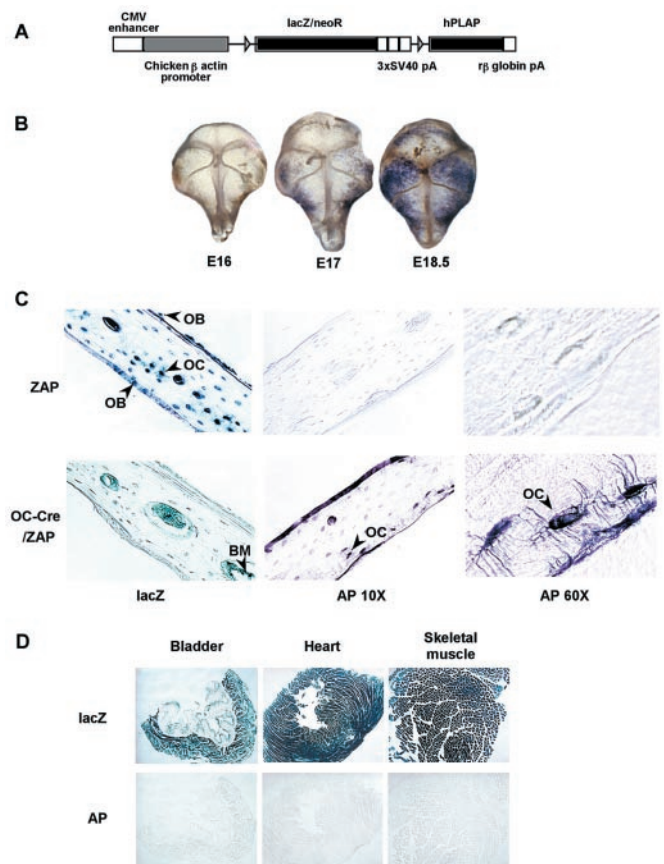


FIG. 2. **Estimation of onset and efficiency of Cre-mediated recombination levels in mouse tissues.** *A*, diagram of the Z/AP transgene construct revised from Ref. 22. The positions and the orientation of two *loxP* sites are indicated by gray triangles. *B*, whole mount calvaria from E16, 17, and 18.5 OC-*Cre*/Z/AP embryos stained for alkaline phosphatase. AP-positive cells are absent in E16 calvaria but clearly present in E17 calvaria at primary ossification centers. *C*, X-gal- and alkaline phosphatase-stained calvarial sections ($\times 10$ magnification) from the Z/AP mouse (ZAP) and from offspring of OC-*Cre* and Z/AP double transgenic mice (line 6). Calvaria derived from offspring from OC-*Cre*/Z/AP crosses demonstrated a marked reduction in X-gal staining and the appearance of AP in the cells of the osteoblast lineage. The far right panel shows a higher magnification ($\times 60$) of the alkaline phosphatase-positive osteocytes in calvaria from the OC-*Cre*/Z/AP mice. *D*, representative non-skeletal tissue sections of the OC-*Cre* and Z/AP double transgenic mouse from OC-*Cre* line 6.

stained for X-gal, to estimate the efficiency of Cre-mediated recombination. Osteoblasts, osteocytes, lining cells and cells within the marrow cavities of calvaria from Z/AP embryos consistently stained positive for X-gal and were AP-negative (Fig. 2C). In contrast, calvaria derived from OC-*cre*/Z/AP double transgenics exhibited a marked reduction in X-gal staining and the appearance of AP staining in the cells of the osteoblast lineage (Fig. 2C; the latter staining was less uniform than that for X-gal, possibly due to less efficient penetration of the AP reaction reagents into the whole mount preparation). In the double transgenic embryos, cells within the marrow (likely representing derivatives of hematopoietic origin) continued to stain positive for X-gal.

To also provide an approximate quantitative estimate for the degree of Cre-mediated DNA excision brought about by the OC-*cre* transgene (“excision index”), we counted the numbers of X-gal-positive osteoblasts and osteocytes in calvarial sections from OC-*cre*/Z/AP and Z/AP (control) mice (4 sections each). We found that $84.4 \pm 0.7\%$ of the cells being monitored (2752 of 3261 cells) were positive for β -galactosidase expression in the control mice, whereas the corresponding score in the double

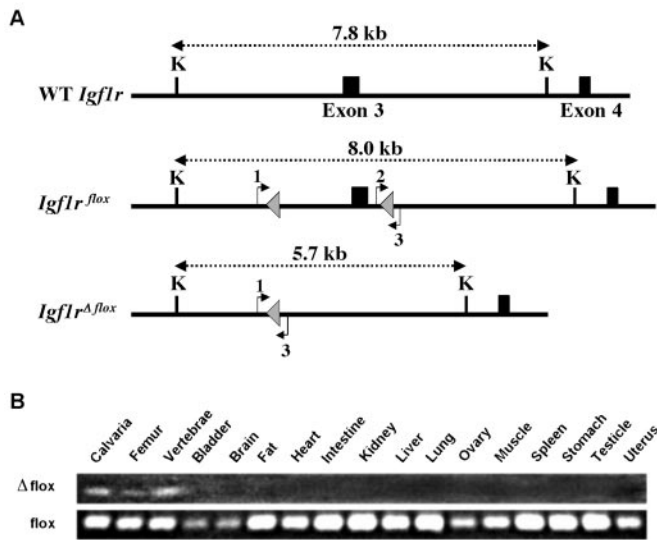


FIG. 3. Osteoblast-specific Cre-mediated recombination in homozygous *Igf1r^{flox/flox}* conditional mutant mice also carrying an *OC-cre* transgene. *A*, partial restriction map in the region of exons 3 and 4 (black rectangles) of the wild-type (WT) mouse *Igf1r* locus. Conditional mutant alleles before and after Cre-mediated excision of exon 3 and flanking sequences (*Igf1r^{flox}* and *Igf1r^{Δflox}*, respectively) are shown. The *floxP* sites (gray triangles) are not in scale. The sizes of the *KpnI* (K) DNA fragments and the positions of primers (1, 2, and 3) used for PCR analysis (for details, see “Materials and Methods”) are indicated. *B*, PCR analysis of Cre-mediated recombination in organs from a Δ *Igf1r* mouse. PCR analysis was performed using DNA templates from tissues of Δ *Igf1r* mice offspring as described under “Materials and Methods.” The top panel shows the PCR fragment generated by primers 1 and 3 specific for the recombined allele (Δ *flox*). Recombination was detected only in skeletal tissue. The bottom panel shows the PCR fragment generated by primers 2 and 3 specific for the non-recombined allele (*flox*).

Δ transgenic calvarial sections was only $9.8 \pm 1.4\%$ (248 of 2530 cells). Thus, the estimated excision index in osteoblasts and osteocytes was $[1-(9.8/84.4)] \times 100$ or 88.4%. Non-skeletal tissues including bladder, heart, and skeletal muscle from the same *OC-cre/Z/AP* mice consistently stained positive for lacZ and negative for AP (Fig. 2D). Moreover, PCR analysis using DNA templates from tissues of *OC-cre/Igf1r^{flox/flox}* offspring confirmed that Cre-mediated recombination occurred exclusively in bone (Fig. 3B).

Despite the fact that a direct estimation of the excision index for the *Igf1r^{flox}* allele in osteoblasts and osteocytes is not feasible, we believe that assigning a level of nearly 90% by extrapolation from the results with the Z/AP reporter (documenting the successful performance of the *OC-cre* transgene) is justifiable, on the basis of the following consistent results. Whenever the *Igf1r^{flox}* locus was used in combination with various high-performance *cre* transgenes analogous to *OC-cre*, including a liver-specific albumin-*cre* (5), a brain-specific CaMKII α -*cre* (30), a pancreatic β -cell-specific RIP-*cre* (31), and a mammary gland-specific WAP-*cre* (32), practically complete Cre-mediated recombination has been observed.³

Bone Abnormalities Resulting from Osteoblast-specific Disruption of the *Igf1r* Gene—Among the progeny of crosses between *OC-cre/Igf1r^{+flox}* and *Igf1r^{flox/flox}* mice, female animals with an *OC-cre/Igf1r^{flox/flox}* genotype were selected for a detailed study of mutational effects using the femur as a long bone representative, whereas their *Igf1r^{flox/flox}* female siblings served as controls. The abnormalities described below were qualitatively similar, but less pronounced in male experimen-

tal animals (data not shown). Because of the expression of the *cre* transgene from E17 onward, osteoblasts appearing for the first time postnatally in the long bones of *OC-cre/Igf1r^{flox/flox}* mice possess an *Igf1r^{Δflox/Δflox}* mutant genotype. For simplicity, these experimental animals will be referred to below as Δ *Igf1r* mice, although in all cells other than osteoblasts the floxed alleles of the *Igf1r* gene remain intact. Also by convention, the genetically modified, but normal (control) mice will be considered as indistinguishable from wild-type.

To assess quantitatively bone mass, architecture, and turnover, static and dynamic histomorphometric analyses were performed on female Δ *Igf1r* and control littermates at 3 and 6 weeks of age, when the skeletal modeling in the mouse is very active (33). At these ages, the mutant and normal animals were indistinguishable in size and weight. Moreover, no differences in femoral lengths were detected at 6 weeks (measured in mm with a dial caliper; 14.31 ± 0.45 and 14.41 ± 0.34 for Δ *Igf1r* and control female mice, respectively, with corresponding values for males of 15.18 ± 0.46 and 15.0 ± 0.53). Thus, disruption of the *Igf1r* gene in osteoblasts did not appear to affect the overall postnatal growth in the mutants.

Although the 6-week measurements were focused on the secondary spongiosa of the distal femur, the histomorphometric analysis at 3 weeks was performed on the femoral epiphysis because at this age there is a greater amount of bone at this site (Table I). These quantitative data, which were consistent with qualitative evaluations of the trabecular bone in the primary and secondary spongiosa, revealed that the rate of epiphyseal bone formation (normalized for bone surface) was dramatically reduced in Δ *Igf1r* mice (~42% of normal; Table I and Fig. 4). Moreover, significant reductions in osteoblast and osteoclast numbers per bone perimeter (67–69% of normal) were observed (Table I and Fig. 4). However, differences between mutants and controls in trabecular bone volume fraction or architecture were not detected at this time point.

Dynamic histomorphometric measurements on 6 week-old mice demonstrated that, in comparison with the controls, the mineral apposition rate was impaired in the Δ *Igf1r* mice, consistent with a dramatic (3-fold) increase in mineralization lag time (Table I and Fig. 5). Similar observations were made in the epiphysis (data not shown). Unexpectedly, however, the amount of osteoid, as indicated by the osteoid-related parameters, was significantly increased in the mutants, and this change was accompanied by an increase in osteoclast erosion surface (Table I and Fig. 5).

In comparison with the normal mice, the mineralization defects in the mutants were reflected in decreases in trabecular bone volume fraction (46%), trabecular thickness (25%), and number (29%), accompanied by an increase in trabecular separation (44%) (Table I and Fig. 6). It is notable that the calvarial cortical thickness was also reduced significantly ($p < 0.01$) in the Δ *Igf1r* mice (~80% of normal; 175 ± 11.1 versus 216 ± 20.1 μ m), although the total number of osteocytes and the lacunae occupancy did not differ from the values seen in controls (data not shown).

To further examine bone architecture, femurs from 6-week-old female Δ *Igf1r* and control mice were compared by three-dimensional measurements using microcomputed tomography (μ CT; Fig. 7). We observed that, in the secondary spongiosa of the distal femur, the normalized cancellous bone volume was ~24% lower than normal in the mutants (Table II and Fig. 7A), reflecting a decrease in the number of trabeculae, the separation of which was significantly increased (Table II and Fig. 7A). In addition, in Δ *Igf1r* mice, trabecular connectivity was 35% lower than normal (Table II). In contrast, cortical bone volume and cortical thickness measured at the mid-shaft of the femur

³ S. Xuan and A. Efstratiadis, unpublished data.

TABLE I
Bone histomorphometry

Bone parameter ^a	3 weeks (epiphysis)			6 weeks (secondary spongiosa)		
	Control (C)	Mutant (M)	M/C ^d	Control	Mutant	M/C ^d
Bone structure						
Bone volume/tissue volume (BV/TV; %)	3.08 ± 0.75	2.47 ± 0.49		5.73 ± 0.65	3.09 ± 0.34 ^c	53.9
Trabecular thickness (Tb.Th; μm)	19.0 ± 1.8	20.5 ± 1.3		22.3 ± 1.56	16.8 ± 0.65 ^c	75.3
Trabecular number (Tb.N; /mm)	1.51 ± 0.24	1.19 ± 0.21		2.58 ± 0.23	1.83 ± 0.17 ^b	70.9
Trabecular separation (Tb.Sp; μm)	753 ± 127	980 ± 158		388 ± 37	557 ± 47 ^b	143.6
Bone formation						
Osteoid volume/bone volume (OV/BV; %)	3.43 ± 0.76	2.84 ± 1.2		4.93 ± 0.97	8.36 ± 1.08 ^b	169.6
Osteoid surface/bone surface (OS/BS; %)	17 ± 3.58	11.86 ± 2.48		20.65 ± 2.97	29.82 ± 1.99 ^b	144.4
Osteoid thickness (O.Th; μm)	3.01 ± 0.39	3.06 ± 1.12		3.54 ± 0.29	3.84 ± 0.35	
Osteoblast surface/bone surface (Ob.S/BS; %)	22.5 ± 2.28	13.8 ± 1.94 ^b	61.3	17.9 ± 3.12	26.0 ± 1.89 ^b	145.3
Osteoblast number/bone perimeter (NOB/BPm; no./100 mm)	1498 ± 116	1039 ± 128 ^b	69.4	1364 ± 248	1833 ± 121	
Bone erosion						
Erosion surface/bone surface (ES/BS; %)	14.1 ± 1.68	12.0 ± 1.48		14.0 ± 2.3	25.9 ± 2.47 ^c	185.0
Erosion depth (E.De; μm)	5.83 ± 0.4	7.91 ± 1.59		5.31 ± 0.6	4.87 ± 0.36	
Osteoblast surface (Oc.S/BS; %)	6.87 ± 0.95	4.8 ± 0.87		7.97 ± 0.69	11.6 ± 2.53	
Osteoclast number/bone perimeter (NOc/BPm; no./100 mm)	232 ± 21	156 ± 20 ^b	67.2	290 ± 38	418 ± 98	
Bone dynamics						
Mineral apposition rate (MAR; μm/day)	2.91 ± 0.17	2.41 ± 0.44 ^b	82.8	3.36 ± 0.27	2.57 ± 0.2 ^b	76.5
Mineralizing surface/bone surface (MS/BS; %)	27.3 ± 5.51	14.7 ± 2.3		16.1 ± 2.29	14.6 ± 2.71	
Bone formation rate/bone surface (BFR/BS; mm ³ /cm ² /yr)	34.3 ± 4.86	14.3 ± 4.37 ^b	41.7	19.4 ± 2.91	13.8 ± 2.55	
Mineralization lag time (Mlt; day)	0.8 ± 0.2	1.95 ± 0.83		1.85 ± 0.39	5.58 ± 1.75 ^b	301.6

^a Values are shown as mean ± S.E. ($n = 7$ per group at 3 weeks; $n = 8$ per group at 6 weeks).

^b $p < 0.05$.

^c $p < 0.01$.

^d Mutant to control ratios (M/C; expressed as percentages) are shown only for values exhibiting statistically significant differences.

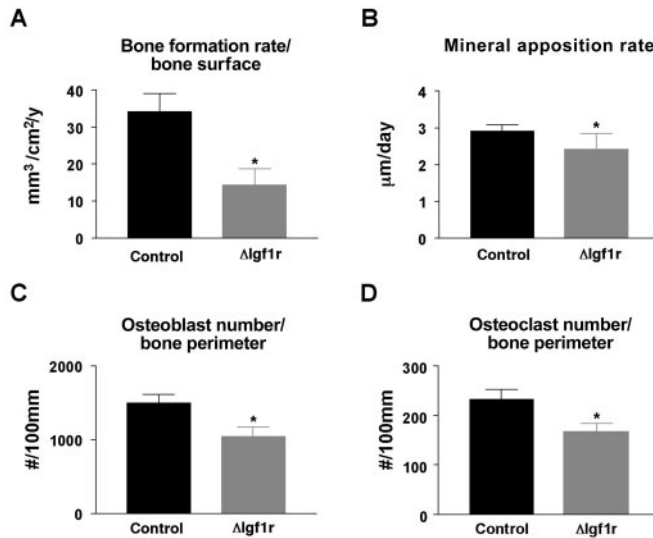


FIG. 4. **Disruption of the *Igf1r* reduces bone formation rate.** Three-week-old female mice were labeled with sequential doses of calcein and dynamic indices of bone formation were quantitated in epiphyseal trabeculae of the femur of female control (black bars, $n = 7$) and $\Delta Igf1r$ mice (gray bars, $n = 7$) as described under "Materials and Methods." Data represent mean ± S.E. *, $p < 0.05$.

were not significantly different between the two animal groups.

Despite differences in the magnitude of relative values (mutant to normal ratios) between the results obtained by histological or μ CT analyses, the two sets of data are consistent in the conclusions that can be drawn from the parameters measured, with a single exception. Whereas trabecular thickness assessed by histomorphometry was significantly reduced in the mutants, no change was detected by μ CT. This is probably due to lower resolution ($\sim 12 \mu\text{m}$ in μ CT measurements versus 3–4 μm in histology) that could lead to overestimates in thickness. An additional factor related to numerical differences between the two methods was the use of dissimilar algorithms in the respective computations (whereas a plate-like bone structure

was assumed for histomorphometry, a model-independent algorithm was used for evaluation of microarchitecture by μ CT).

DISCUSSION

We have provided strong genetic evidence demonstrating for the first time that IGF signaling in cells of the osteoblastic lineage is essential for maintenance of the mineralization process at a normal level. Despite significant complexities concerning the exact roles of the IGFs in bone formation and remodeling (7), this conclusion can be clearly reached, based on the following considerations about the particular experimental design that we used.

In the mutant mice that we have generated and examined, all components of the IGF system have remained intact with the exception of differentiating osteoblasts, in which the function of the receptor mediating the signaling of IGF ligands was selectively ablated. In fact, because of the commencement of Cre-mediated recombination at E17, at least as assayed in primary ossification centers of the calvaria by using *Z/AP* reporter mice, we can infer that all descendants of osteoblastic cells lacking IGF1R were unable to respond to stimuli from the cognate ligands during their subsequent developmental history. In this regard, the validity of our conclusions is independent of the particular mode of action of the IGFs (local and/or systemic) and of the exact contribution of either one of these growth factors, which apparently play non-overlapping roles that are not always concurrent (IGF1 acts throughout both embryonic and postnatal development, whereas IGF2 acts only during embryogenesis) (34). These considerations permit the direct establishment of a cause/effect relationship correlating the absence of events in the IGF1R signaling cascade with the phenotypic manifestations of the osteoblast-specific mutation, as reflected in the structural and functional bone features that were evaluated by histomorphometry and μ CT.

Although the mechanistic aspects of our observations are currently unclear, and a considerable amount of future work will be necessary to even begin understanding at a more reductionist level functional relationships and their potential rele-

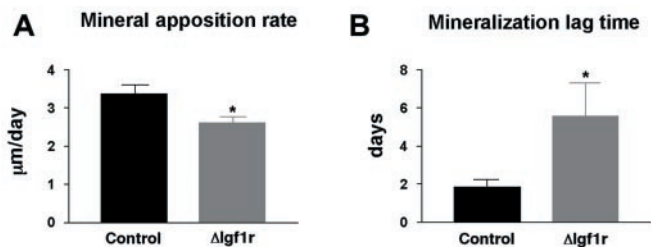
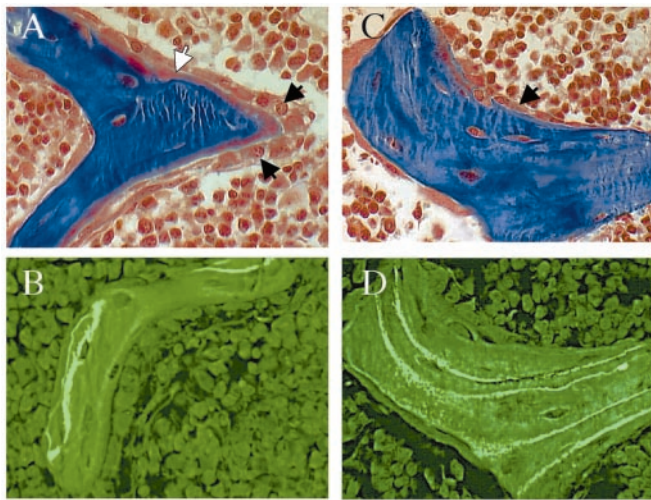


FIG. 5. Impaired mineralization of bone matrix in the $\Delta Igf1r$ mice. *Top panel*, six-week-old female mice were labeled with sequential doses of calcein and dynamic indices of bone formation were quantitated in metaphyseal trabeculae of the femur as described under "Materials and Methods." *Panels A and C* show H+E stained sections of mutant (*left*) and control (*right*) mouse femurs. An increase in the amount of osteoid (*white arrow*) and size and number of osteoblasts (*black arrows*) is apparent in the bone from the $\Delta Igf1r$ mice. *Panels B and D* show representative calcein-labeled sections of distal femur from mutant (*left*) and control (*right*) mice. *Bottom panel*, mineralization apposition rate and mineralization lag time in female control (*black bars*, $n = 10$) and $\Delta Igf1r$ mice (*gray bars*, $n = 8$). Data represent mean \pm S.E. *, $p < 0.05$.

vance to the pathophysiology of osteoporosis (35), the particular mouse model that we have described would greatly simplify further investigations, as it has brought into sharp focus events downstream from the activation of IGF1R, which can be studied separately from the involvement of upstream stimuli.

At present, the available comparative data of bone phenotypic features in $\Delta Igf1r$ mice at around weaning (3 weeks) and at a time past puberty (6 weeks), when growth has significantly progressed and the animals are approaching a period toward a steady-state, should be evaluated with caution, pending a more detailed developmental analysis. Nevertheless, our results suggest that, in the earlier period of bone modeling at weaning, IGF signaling is necessary for sustaining in osteoblasts proliferative and/or anti-apoptotic events at normal levels, as evidenced by a reduction in osteoblast numbers and a decline in bone formation rate. In addition, apparently because of coupling of osteoblastic and osteoclastic activities, the number of osteoclasts is also reduced. Surprisingly, this trend did not continue, and at 6 weeks of age statistically significant differences in osteoblast/osteoclast numbers were not observed between mutants and controls (in fact, the absolute cell numbers were higher in the mutants, perhaps providing a clue about potential compensatory effects). Moreover, an unexpected excess in the amount of uncalcified osteoid (osteoidosis) was detected that was accompanied by a defect in mineralization. In addition, the skeletal properties representing bone quality indicated the presence of bone microarchitectural abnormalities,

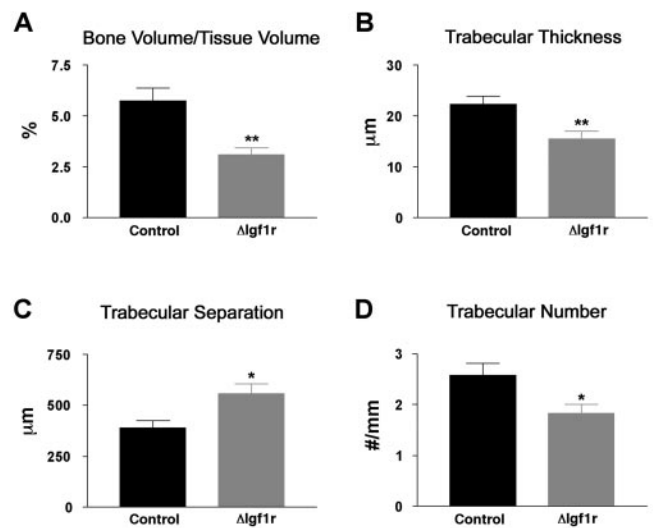


FIG. 6. Decreased bone volume in $\Delta Igf1r$ mice. Quantitative histomorphometric measurements were performed at the distal femur of 6-week-old female control (*black bars*, $n = 10$) and $\Delta Igf1r$ mice (*gray bars*, $n = 8$) as described under "Materials and Methods." Data represent mean \pm S.E. *, $p < 0.05$; **, $p < 0.01$.

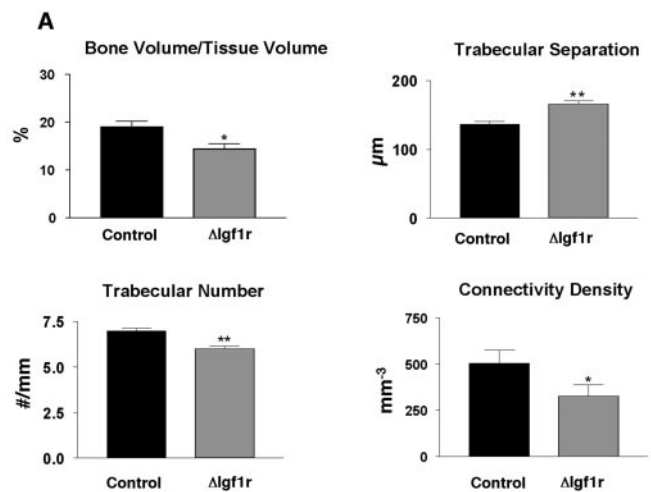


FIG. 7. Changes in bone microarchitecture in $\Delta Igf1r$ mice. Micro CT analysis was performed at the distal femur of 6-week-old female $\Delta Igf1r$ and control mice. *A*, values of trabecular bone volume, trabecular separation, number, and connectivity density of control (*black bars*, $n = 7$) and $\Delta Igf1r$ mice (*gray bars*, $n = 9$). Data represent mean \pm S.E. *, $p < 0.05$; **, $p < 0.01$. *B*, representative three-dimensional images of distal femur from a control and a $\Delta Igf1r$ mouse at 34-micron resolution. *Inset* shows reconstructed trabecular bone images at 9-micron resolution.

which were revealed as reductions in the number, thickness and extent of attachment (connectivity) of trabeculae, with concomitant increase in trabecular spacing and lower than

TABLE II
 μ CT analysis (distal femur)

Bone site and parameter	Control (C); <i>n</i> = 7	Mutant (M); <i>n</i> = 9	M/C
			%
Whole femur			
Bone volume (BV; mm ³)	18.96 ± 0.7 ^a	17.94 ± 0.65	
Apparent volume density (AVD; %)	62.3 ± 1.2	59.3 ± 0.9	
Distal femur (cancellous bone)			
Bone volume/tissue volume (BV/TV; %)	19.0 ± 1.2	14.4 ± 1.1 ^b	75.8
Trabecular thickness (Tb.Th; μ m)	34.0 ± 1.0	34.0 ± 2.0	
Trabecular separation (Tb.Sp; μ m)	137 ± 4	165 ± 5 ^c	120.4
Trabecular number (Tb.N; mm ⁻¹)	7.00 ± 0.14	6.00 ± 0.14 ^c	85.7
Connectivity density (mm ⁻³)	503.8 ± 75.0	327.8 ± 62.4 ^b	65.1
Mid-diaphysis (cortical bone)			
Bone volume (BV; mm ³)	0.537 ± 0.025	0.506 ± 0.026	
Cortical thickness (μ m)	187 ± 7	178 ± 6	

^a Values are shown as mean ± S.E.

^b *p* < 0.05.

^c *p* < 0.01.

normal bone density (measured as BV/TV). Importantly, however, the absence of histopathological findings, such as tissue disorganization, indicated that the overall bone morphogenetic processes were not perturbed in Δ *Igf1r* mice. Among other possibilities, the osteoidosis occurring in combination with reduced mineralization may reflect compensatory attempts by substitute signaling systems. Alternatively, the detected changes may represent different consequences of the lack of IGF signaling appearing specifically at the more advanced developmental time of 6 weeks, when the remodeling process has been intensified. It is notable, in this regard, that cortical bone volume was not significantly affected in the mutants, whereas the pronounced effects on trabecular bone could be explained by the fact that this skeletal compartment is subject to the highest rate of remodeling, particularly over the time period of the observations (6 weeks).

Our data indicate that, despite a high degree of coordination, the processes of osteoid production on one hand and mineralization on the other are dissociable and can be viewed as outcomes of two separate processes. During bone formation, osteoblasts not only synthesize, secrete and deposit collagen I and noncollagenous proteins of the extracellular matrix (osteoid), but also participate in the mineralization process, which continues to remain poorly understood (36–38). After budding and pinching off of matrix vesicles containing hydroxyapatite from the surface of osteoblasts, the mineral crystals are first exposed by breakdown of the membrane that surrounds them, and are then progressively enlarged in the extracellular matrix. It is thought that the latter process is controlled by the osteoblasts themselves through an adjustment of the extracellular ionic conditions. The most sensitive index for detecting a mineralization defect is an increase in the lag time between osteoid deposition and mineral addition. This “mineralization lag time” (also called “osteoid maturation period”), which is increased 3-fold over normal in the Δ *Igf1r* mutant mice, is apparently required for some modification of the osteoid to become competent for support of mineralization. Thus, the normal balance between the rates of osteoid production/maturation and mineralization appears to be significantly perturbed in the absence of IGF signaling, as if there is an incomplete block in some feed-back loop affecting the cross-talk between the corresponding putative pathways. We propose that this causes a temporal uncoupling between the phases of ossification, thus, resulting in osteoidosis and poor mineralization.

It remains to be seen whether previous circumstantial evidence suggesting that IGF1 could modulate bone mineralization is mechanistically relevant to our observations. It was reported, for example, that IGF1 levels in conditioned medium

of primary rat osteoblasts *in vitro* rise in association with bone nodule formation (11), while infusions of an IGF1/IGFBP-3 complex into 6-week-old rats resulted in a doubling of the exchangeable calcium pool in bone compared with saline-treated controls (39). It is also notable that inorganic phosphate transport is thought to drive accumulation of mineral inside the matrix vesicles and to be pivotal in the induction of the calcification process (40). In this regard, it is intriguing that IGF1 has been shown to stimulate inorganic phosphate transport in human osteoblastic cells (SaOS2) by inducing the expression of a sodium-dependent phosphate transporter (Glv-1) (41). It is possible, therefore, that IGF1 is required for adequate phosphate uptake by osteoblasts.

Regardless of mechanisms, the evidence that we have presented is likely to have important clinical implications. Thus, while it is generally acknowledged that IGF1 is critical for both linear bone growth and skeletal acquisition, our findings suggest that IGF1 is essential for coupling matrix biosynthesis to sustained mineralization. This action could be particularly important during the pubertal growth spurt when rapid bone formation and consolidation are required.

Acknowledgments—We thank Chris Langub and William Stuart for assistance in preparing the article.

REFERENCES

1. Efstratiadis, A. (1998) *Int. J. Dev. Biol.* **42**, 955–976
2. Lupu, F., Terwilliger, J. D., Lee, K., Segre, G. V., and Efstratiadis, A. (2001) *Dev. Biol.* **229**, 141–162
3. Baserga, R., Resnicoff, M., D'Ambrosio, C., and Valentinis, B. (1997) *Vitam. Horm.* **53**, 65–98
4. Nakae, J., Kido, Y., and Accili, D. (2001) *Endocr. Rev.* **22**, 818–835
5. Yakar, S., Liu, J. L., Stannard, B., Butler, A., Accili, D., Sauer, B., and LeRoith, D. (1999) *Proc. Natl. Acad. Sci. U. S. A.* **96**, 7324–7329
6. D'Ercole, A. J., and Calikoglu, A. S. (2001) *Growth Horm. IGF Res.* **11**, 261–265
7. Conover, C. A. (2000) *Growth Horm. IGF Res.* **10**, Suppl. B, S107–S110
8. Shinar, D. M., Endo, N., Halperin, D., Rodan, G. A., and Weinreb, M. (1993) *Endocrinology* **132**, 1158–1167
9. Wang, E., Wang, J., Chin, E., Zhou, J., and Bondy, C. A. (1995) *Endocrinology* **136**, 2741–2751
10. Canalis, E. (1993) *Bone* **14**, 273–276
11. Birnbaum, R. S., Bowsher, R. R., and Wren, K. M. (1995) *J. Endocrinol.* **144**, 251–259
12. Parfitt, A. M., Mundy, G. R., Roodman, G. D., Hughes, D. E., and Boyce, B. F. (1996) *J. Bone Miner. Res.* **11**, 150–159
13. Hughes, D. E., and Boyce, B. F. (1997) *Mol. Pathol.* **50**, 132–137
14. Hill, P. A., Tumber, A., and Meikle, M. C. (1997) *Endocrinology* **138**, 3849–3858
15. Hill, P. A., Reynolds, J. J., and Meikle, M. C. (1995) *Endocrinology* **136**, 124–131
16. Olsen, B. R., Reginato, A. M., and Wang, W. (2000) *Annu. Rev. Cell Dev. Biol.* **16**, 191–220
17. Karsenty, G., and Wagner, E. F. (2002) *Dev. Cell* **2**, 389–406
18. Zhao, G., Monier-Faugere, M. C., Langub, M. C., Geng, Z., Nakayama, T., Pike, J. W., Chernausek, S. D., Rosen, C. J., Donahue, L. R., Malluche, H. H., Fagin, J. A., and Clemens, T. L. (2000) *Endocrinology* **141**, 2674–2682
19. Liu, J. P., Baker, J., Perkins, A. S., Robertson, E. J., and Efstratiadis, A. (1993) *Cell* **75**, 59–72

20. Clemens, T. L., Tang, H., Maeda, S., Kesterson, R. A., DeMayo, F., Pike, J. W., and Gundberg, C. M. (1997) *J. Bone Miner. Res.* **12**, 1570–1576
21. Dietrich, P., Dragatsis, I., Xuan, S., Zeitlin, S., and Efstratiadis, A. (2000) *Mamm. Genome* **11**, 196–205
22. Lobe, C. G., Koop, K. E., Kreppner, W., Lomeli, H., Gertsenstein, M., and Nagy, A. (1999) *Dev. Biol.* **208**, 281–292
23. Ruegsegger, P., Koller, B., and Muller, R. (1996) *Calcif. Tissue Int.* **58**, 24–29
24. Alexander, J. M., Bab, I., Fish, S., Muller, R., Uchiyama, T., Gronowicz, G., Nahounou, M., Zhao, Q., White, D. W., Chorev, M., Gazit, D., and Rosenblatt, M. (2001) *J. Bone Miner. Res.* **16**, 1665–1673
25. Pfeilschifter, J., Laukhuf, F., Muller-Beckmann, B., Blum, W. F., Pfister, T., and Ziegler, R. (1995) *J. Clin. Investig.* **96**, 767–774
26. Malluche, H. H., and Faugere, M. C. (1986) *Atlas of Mineralized Bone Histology*, Karger, New York
27. Goldner, J. (1997) *Am. J. Pathol.* **14**, 237–243
28. Malluche, H. H., Sherman, D., Meyer, W., and Massry, S. G. (1982) *Calcif. Tissue Int.* **34**, 439–448
29. Parfitt, A. M., Drezner, M. K., Glorieux, F. H., Kanis, J. A., Malluche, H., Meunier, P. J., Ott, S. M., and Recker, R. R. (1987) *J. Bone Miner. Res.* **2**, 595–610
30. Dragatsis, I., and Zeitlin, S. (2000) *Genesis* **26**, 133–135
31. Herrera, P. L. (2000) *Development* **127**, 2317–2322
32. Ludwig, T., Fisher, P., Murty, V., and Efstratiadis, A. (2001) *Oncogene* **20**, 3937–3948
33. Richman, C., Kutilek, S., Miyakoshi, N., Srivastava, A. K., Beamer, W. G., Donahue, L. R., Rosen, C. J., Wergedal, J. E., Baylink, D. J., and Mohan, S. (2001) *J. Bone Miner. Res.* **16**, 386–397
34. Baker, J., Liu, J. P., Robertson, E. J., and Efstratiadis, A. (1993) *Cell* **75**, 73–82
35. Rizzoli, R., Bonjour, J. P., and Ferrari, S. L. (2001) *J. Mol. Endocrinol.* **26**, 79–94
36. Anderson, H. C. (1995) *Clin. Orthop.* 266–280
37. Boskey, A. L. (1996) *Connect. Tissue Res.* **35**, 357–363
38. Sims, N., and Baron, R. (2000) in *Skeletal Growth Factors* (Canalis, E., ed) pp. 1–16, Lippincott Williams & Wilkins
39. Zhang, Q., Wastney, M. E., Rosen, C. J., and Weaver, C. M. (2001) *J. Bone Miner. Res.* **16**, S356
40. Caverzasio, J., and Bonjour, J. P. (1996) *Kidney Int.* **49**, 975–980
41. Suzuki, A., Palmer, G., Bonjour, J. P., and Caverzasio, J. (2001) *Bone* **28**, 589–594